LETTER

Flexible high–temperature dielectric materials from polymer nanocomposites

Qi Li[1], Lei Chen[1], Matthew R. Gadinski[1], Shihai Zhang[2], Guangzu Zhang[1], Haoyu Li[3], Aman Haque[4], Long–Qing Chen[1], Tom Jackson[3] & Qing Wang[1]

Dielectric materials, which store energy electrostatically, are ubiquitous in advanced electronics and electric power systems[1-8]. Compared to their ceramic counterparts, polymer dielectrics have higher breakdown strengths and greater reliability[1-3,9], are scalable, lightweight and can be shaped into intricate configurations, and are therefore an ideal choice for many power electronics, power conditioning, and pulsed power applications[1,9,10]. However, polymer dielectrics are limited to relatively low working temperatures, and thus fail to meet the rising demand for electricity under the extreme conditions present in applications such as hybrid and electric vehicles, aerospace power electronics, and underground oil and gas exploration[11-13]. Here we describe crosslinked polymer nanocomposites that contain boron nitride nanosheets, the dielectric properties of which are stable over a broad temperature and frequency range. The nanocomposites have outstanding high-voltage capacitive energy storage capabilities at record temperatures (a Weibull breakdown strength of 403 megavolts per metre and a discharged energy density of 1.8 joules per cubic centimetre at 250 degrees Celsius). Their electrical conduction is several orders of magnitude lower than that of existing polymers and their high operating temperatures are attributed to greatly improved thermal conductivity, owing to the presence of the boron nitride nanosheets, which improve heat dissipation compared to pristine polymers (which are inherently susceptible to thermal runaway). Moreover, the polymer nanocomposites are lightweight, photopatternable and mechanically flexible, and have been demonstrated to preserve excellent dielectric and capacitive performance after intensive bending cycles. These findings enable broader applications of organic materials in high-temperature electronics and energy storage devices.

The best commercially available dielectric polymer represented by biaxially oriented polypropylene (BOPP) can operate only at temperatures below 105 °C (ref. 14). Therefore, thermal management is always required to enable the use of dielectric polymers in high-temperature applications. For example, to accommodate BOPP film capacitors in the power inverters of hybrid and electric vehicles, which are used to control and convert direct current from batteries into the alternating current required to power the motor, cooling systems have to be employed to decrease the environmental temperature from about 140 °C to about 70 °C. This brings extra weight, volume and energy consumption to the integrated power system and reduces its reliability and efficiency. The upsurge in lightweight and flexible electronic devices has also created a tremendous demand for high-temperature dielectric polymers, as the heat generated by electronic devices and circuitry increases exponentially with miniaturization and functionality.

A variety of high-performance engineering polymers have been considered as possible high-temperature dielectric materials to address these urgent needs[15-19]. Until now, the key criteria established for evaluating high-temperature dielectric polymers has been the glass transition temperature (T_g) and thermal stability. At temperatures approaching T_g, polymers lose their dimensional and electromechanical stability and display large variations in dielectric constant (K) and dissipation factor (DF) with temperature. Making use only of materials that have high T_g works reasonably well at high temperatures but only under relatively low electric fields and this approach has had very limited success when the material is subject to both high temperatures and high voltages.

Here (see Fig. 1a) we thermally crosslinked divinyltetramethyldisiloxane-bis(benzocyclobutene) (BCB) in the presence of boron nitride nanosheets (BNNSs, Fig. 1b and c) to afford the crosslinked nanocomposite c-BCB/BNNS (Fig. 1f and g, Supplementary Information section 1). BNNSs, which form a wide-bandgap (∼6 eV) insulator with ultrahigh thermal conductivities in the range ∼300–2,000 W m^{-1} K^{-1} (refs 20 and 21), were prepared through liquid-phase exfoliation of hexagonal boron nitride (h-BN) powders[22].

Compared to the crosslinked pristine BCB referred to as c-BCB, the most striking feature of c-BCB/BNNS is substantially suppressed high-field electrical conduction at high temperatures (Supplementary Information sections 2 and 3). For example, the electrical conductivity decreases from 4×10^{-12} S m^{-1} in c-BCB to 9.2×10^{-14} S m^{-1} in c-BCB/BNNS and the conduction loss decreases from 18% in c-BCB to 3% in c-BCB/BNNS under an applied field of 200 MV m^{-1} at 150 °C. Coupled with the higher Young's modulus arising from the introduced BNNSs, which impedes the occurrence of the electromechanical breakdown[23], the largely reduced electrical conduction in c-BCB/BNNS results in a greatly improved Weibull breakdown strength (E_b) at high temperatures. For example, E_b improves from 262 MV m^{-1} for c-BCB to 403 MV m^{-1} for c-BCB/BNNS with 10 vol% BNNSs at 250 °C. We note that polymer nanocomposites were previously designed towards improved capacitive energy storage, including BNNS-containing nanocomposites[24], and were mainly intended for room temperature applications[25]. For example, at E_b = 200 MV m^{-1}, the dielectric loss of the best ferroelectric polymer nanocomposite with BNNSs is 15% at room temperature[24], but this quickly rises to 76% when the temperature is increased to 70 °C (Supplementary Fig. 25).

The dielectric properties of c-BCB/BNNS have been evaluated along with state-of-the-art high-temperature capacitor-grade polymer films including polycarbonate (PC, $T_g \approx 150$ °C), poly(ether ether ketone) (PEEK, $T_g \approx 150$ °C), polyetherimide (PEI, $T_g \approx 217$ °C), fluorene polyester (FPE, $T_g \approx 330$ °C) and polyimide (Kapton PI (from Dupont), $T_g \approx 360$ °C) (Supplementary Table 1). We first examine K and DF as a function of temperature and frequency (Fig. 2, Supplementary Information section 4). At 10^4 Hz, which is the frequency of interest for common power conditioning, a minor variation in K with temperature, that is, <1.7%, is seen in c-BCB/BNNS from room temperature to 300 °C, while FPE, the next-best dielectric investigated in this study, shows a K variation of over 8% at 300 °C

[1]Department of Materials Science and Engineering, The Pennsylvania State University, University Park, Pennsylvania 16802, USA. [2]PolyK Technologies, State College, Pennsylvania 16802, USA. [3]Department of Electrical Engineering, The Pennsylvania State University, University Park, Pennsylvania 16802, USA. [4]Department of Mechanical and Nuclear Engineering, The Pennsylvania State University, University Park, Pennsylvania 16802, USA.
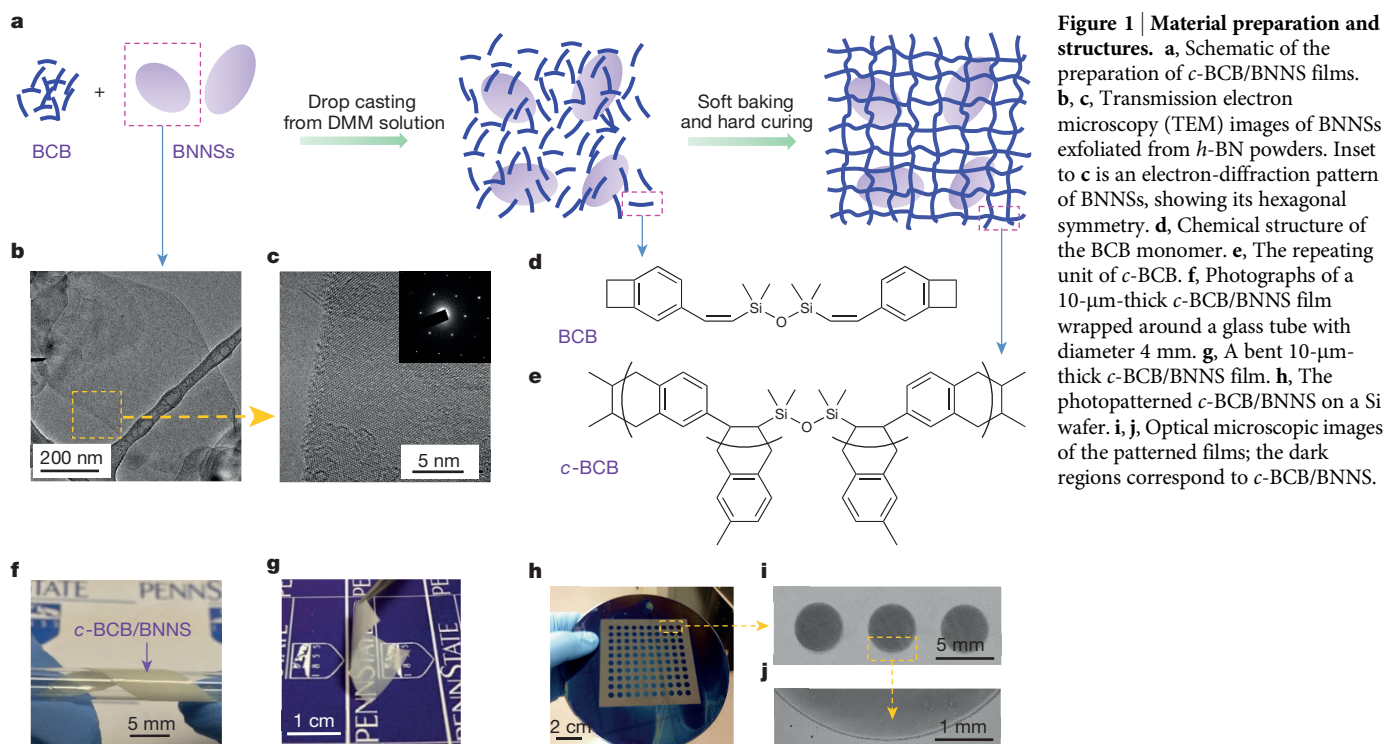
Figure 1 | Material preparation and structures. a, Schematic of the preparation of c-BCB/BNNS films. **b, c**, Transmission electron microscopy (TEM) images of BNNSs exfoliated from h-BN powders. Inset to **c** is an electron-diffraction pattern of BNNSs, showing its hexagonal symmetry. **d**, Chemical structure of the BCB monomer. **e**, The repeating unit of c-BCB. **f**, Photographs of a 10-μm-thick c-BCB/BNNS film wrapped around a glass tube with diameter 4 mm. **g**, A bent 10-μm-thick c-BCB/BNNS film. **h**, The photopatterned c-BCB/BNNS on a Si wafer. **i, j**, Optical microscopic images of the patterned films; the dark regions correspond to c-BCB/BNNS.

relative to room temperature (Supplementary Fig. 15). As presented in Fig. 2c, the temperature coefficient of K for c-BCB/BNNS is around 65 parts per million (p.p.m.) per $°C$, compared to 308 p.p.m. $°C^{-1}$ and 498 p.p.m. $°C^{-1}$ for FPE and Kapton, respectively, within the temperature range 25–300 $°C$. Even under a direct-current bias voltage of 50 MV m^{-1}, the K variation of c-BCB/BNNS is still as low as 1.6% at 250 $°C$, compared to 8.5% for FPE (Supplementary Fig. 15).

Concurrently, the DF value of c-BCB/BNNS at 10^4 Hz only increases from 0.09% to 0.13% with increasing temperature up to 300 $°C$ (Supplementary Fig. 15). Although Kapton shows a stability of DF with temperature under direct-current bias similar to that of c-BCB/BNNS, appreciable increases in DF have been observed in all the other polymer dielectrics. For example, the DF of FPE jumps from 0.22% at room temperature to 1.35% at 280 $°C$. It is also evident that, of
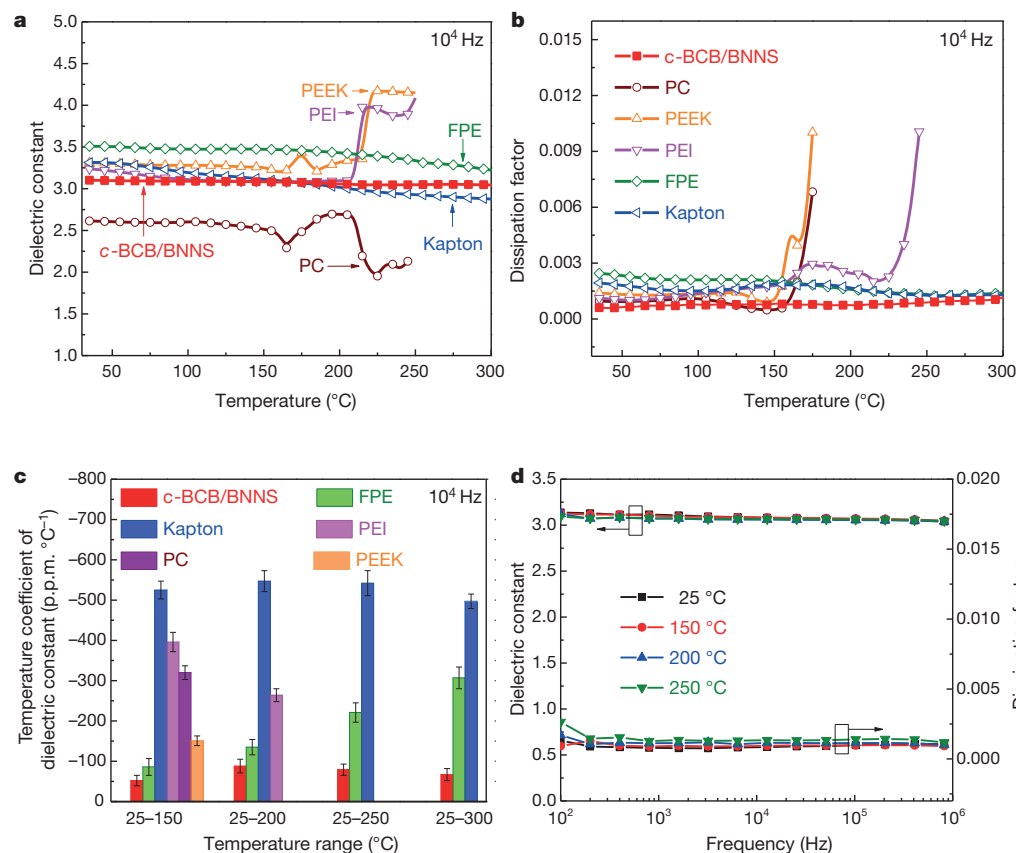

Figure 2 | Dielectric stability.
a, Temperature dependence of dielectric constant. **b**, The DF of c-BCB/BNNS with 10 vol% of BNNSs and high-T_g polymer dielectrics. **c**, Temperature coefficient of the dielectric constant of c-BCB/BNNS with 10 vol% of BNNSs and high-T_g polymer dielectrics at various temperature ranges. **d**, Frequency dependence of the dielectric constant and DF of c-BCB/BNNS with 10 vol% of BNNSs at different temperatures. Error bars show standard deviation.
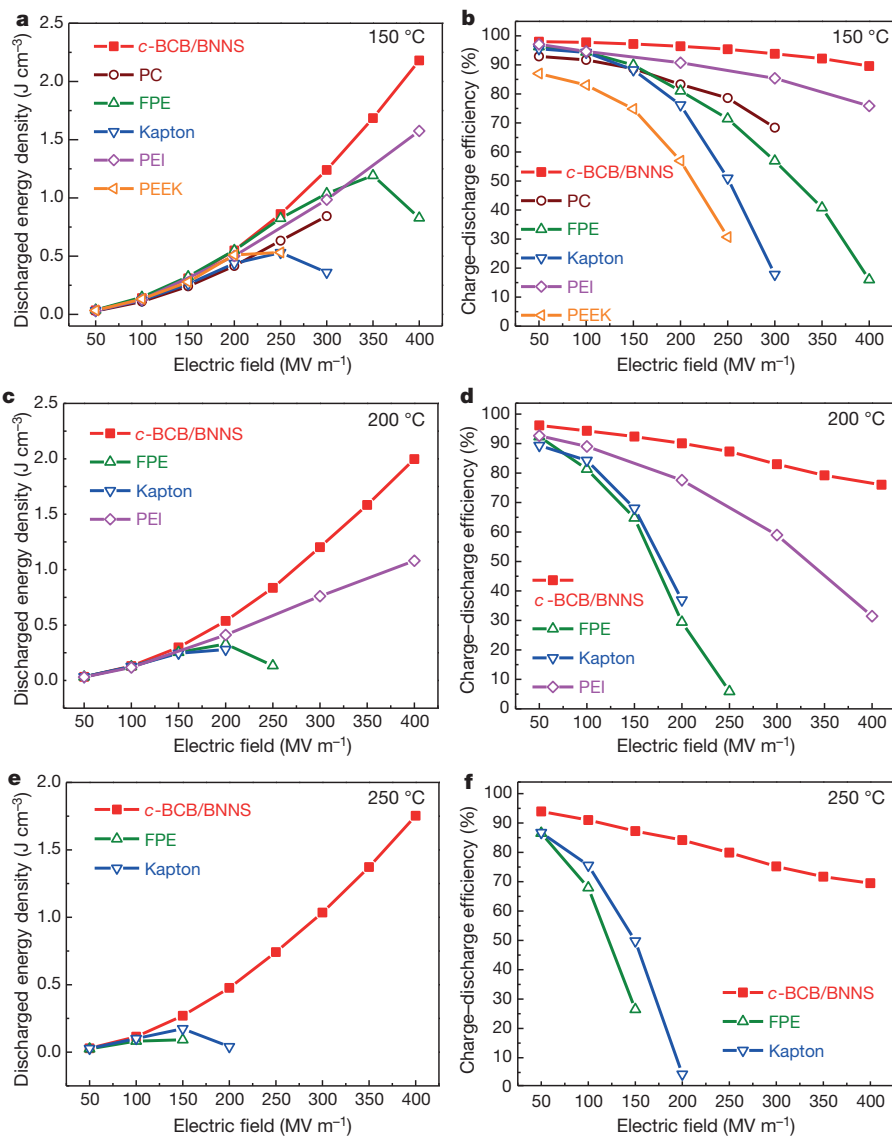
Figure 3 | Electrical energy storage capability. Discharged energy density and charge–discharge efficiency of *c*-BCB/BNNS with 10 vol% of BNNSs and high-T_g polymer dielectrics measured at 150 °C (**a**, **b**), 200 °C (**c**, **d**) and 250 °C (**e**, **f**).

the dielectrics assessed, *c*-BCB/BNNS offers the most stable K and DF in the frequency range 10^2–10^6 Hz at high temperatures (Fig. 2d, Supplementary Figs 16 and 17).

We next studied high-field capacitive energy storage properties at high temperatures (Supplementary Information section 5). As summarized in Fig. 3, *c*-BCB/BNNS clearly outperforms all the high-T_g polymer dielectrics at temperatures ranging from 150 °C to 250 °C in terms of the discharged energy density (U_e) and the charge–discharge efficiency (η). For example, *c*-BCB/BNNS can discharge a U_e exceeding 2.2 J cm^{-3} under 400 MV m^{-1} with a η of larger than 90% at 150 °C. At 200 °C, *c*-BCB/BNNS delivers a U_e of 2 J cm^{-3} under 400 MV m^{-1}, which is twice that of PEI, accompanied by a η value more than 1.5 times higher than that of PEI. As the temperature is further raised to 250 °C, where none of the high-T_g polymer dielectrics can operate at more than 150 MV m^{-1}, *c*-BCB/BNNS is functional up to 400 MV m^{-1} with a U_e of ~1.8 J cm^{-3}. Remarkably, at 200 MV m^{-1}, which is the operating condition of BOPP film capacitors in electric vehicles[26], the value of η for *c*-BCB/BNNS at 150 °C—that is, ~97%—is the same as that of BOPP at 70 °C (Supplementary Fig. 24). This indicates that, by replacing BOPP with *c*-BCB/BNNS, the complex cooling system for power inverters in electric vehicles could be eliminated. Furthermore, under these conditions, the U_e of *c*-BCB/BNNS is over 40% higher than that of BOPP owing to its higher K; that is, 3.1, versus 2.2 for BOPP.

The superior performance of *c*-BCB/BNNS over the high-T_g polymer dielectrics stems from its substantially reduced high-field leakage

current at elevated temperatures. For example, at 200 °C and a field of 200 MV m^{-1}, a current density of 4.2×10^{-8} A cm^{-2} is found in *c*-BCB/BNNS, which is nearly one order of magnitude lower than that of PEI and two orders of magnitude smaller than those of FPE and Kapton (Supplementary Fig. 28). It is important to note that the electrical conduction not only accounts for dielectric loss, which degrades U_e and η, but also generates Joule heating within dielectrics[27]. Depending on the heat dissipation (which is determined primarily by the thermal conductivity of the dielectrics), the geometry of the capacitors, and the cooling systems, the steady-state internal temperature of capacitors could exceed the T_g or even the decomposition temperature of dielectric polymers and cause capacitor failure.

We simulate the steady-state internal temperature distribution of the dielectric films by using finite element computations[28] (Methods, Supplementary Information section 6). As summarized in Supplementary Tables 4–6, it can be seen that the steady-state internal temperatures of *c*-BCB/BNNS film are consistently much lower than those of the high-T_g polymers operating under the same conditions, owing to a pronounced reduction in conduction loss and a marked enhancement in thermal conductivity, that is, from ~0.2 W m^{-1} K^{-1} for the polymers to 1.8 W m^{-1} K^{-1} for *c*-BCB/BNNS. As exemplified in Fig. 4, under a forced convection with air (convective heat transfer coefficient $h = 35$) and an ambient temperature of 200 °C, the PEI-, FPE- and Kapton-based film capacitors are overheated, with temperatures at the film centres of 219 °C, 361 °C, and 435 °C, respectively, at 200 MV m^{-1}.
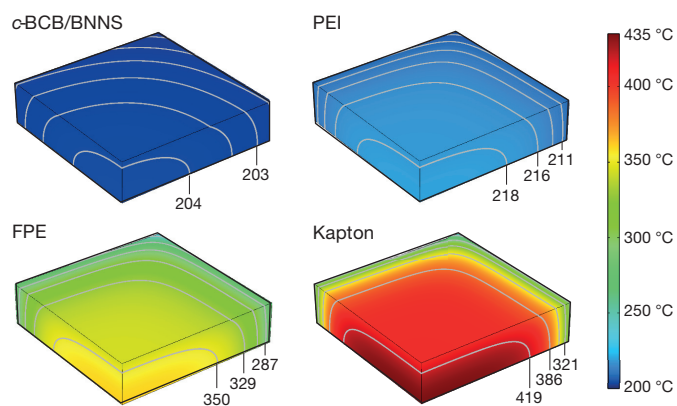
Figure 4 | Steady-state temperature distribution. Simulated steady-state temperature distribution in spiral-wound film capacitors of $40 \times 40 \times 10$ mm^3 enclosure size, based on c-BCB/BNNS with 10 vol% of BNNSs, PEI, FPE and PI (Kapton), respectively, given continuous operation under an electric field of 200 MV m^{-1}, with an ambient temperature of $200\,^\circ$C and a convective heat transfer coefficient of 35. As the model is symmetric in three Cartesian coordinates, only 1/8 of the volume is shown, to expose the centre part of the capacitor.

In contrast, the highest temperature inside c-BCB/BNNS is only $204\,^\circ$C. With the field increasing to 300 MV m^{-1} and 400 MV m^{-1}, the temperatures at the film centre of c-BCB/BNNS are $213\,^\circ$C and $255\,^\circ$C, respectively, still below its T_g ($>350\,^\circ$C), when $h = 200$. Notably, even at $250\,^\circ$C and with active liquid cooling, c-BCB/BNNS is operable at 300 MV m^{-1} with a maximum internal temperature of $308\,^\circ$C. Under high-voltage cycling conditions, it is in fact thermal runaway[29] that dictates the maximum operation field of dielectric polymers and thus acts as the limiting factor of high-field capacitive energy storage at elevated temperatures. Despite high T_g and excellent thermal stability from engineering polymers, their well documented poor thermal conductivities[30] seriously limit the actual working temperatures of capacitors under high fields.

Finally, we demonstrate that c-BCB/BNNS can be readily prepared by photo-polymerization of solution-cast films, which, upon further curing, are found to possess essentially the same dielectric properties as the thermally crosslinked films (see Methods and Supplementary Fig. 27). The ultraviolet-induced crosslinking through an optical mask enables direct photopatterning of c-BCB/BNNS films (Figs 1h–j); this is highly desirable in device fabrications. Furthermore, no degradation in dielectric stability, U_e and η of c-BCB/BNNS measured at room temperature and $250\,^\circ$C was observed after rigorous winding and bending tests (Supplementary Information section 7 and Supplementary Video). This suggests that this nanocomposite may be used in practical flexible electronics and high-throughput roll-to-roll processing into wound cells. Also, it is noteworthy that c-BCB/BNNS has the lowest mass density (~1.10 g cm^{-3}) of the polymer dielectrics studied (Supplementary Table 1). This desirable combination of processibility, flexibility, light weight, and dielectric and capacitive performance in such nanocomposites may transform the way compact power modules and power circuits targeted for harsh environment applications are built.

Online Content Methods, along with any additional Extended Data display items and Source Data, are available in the online version of the paper; references unique to these sections appear only in the online paper.

1. Sarjeant, W. J., Zirnheld, J. & MacDougall, F. W. Capacitors. *IEEE Trans. Plasma Sci.* **26,** 1368–1392 (1998).
2. Sarjeant, W. J., Clelland, I. W. & Price, R. A. Capacitive components for power electronics. *Proc. IEEE* **89,** 846–855 (2001).
3. Tan, Q., Irwin, P. & Cao, Y. Advanced dielectrics for capacitors. *IEEJ Trans. Fund. Mater.* **126,** 1152–1159 (2006).
4. Irvine, J. T. S., Sinclair, D. C. & West, A. R. Electroceramics: characterization by impedance spectroscopy. *Adv. Mater.* **2,** 132–138 (1990).
5. Reaney, I. M. & Iddles, D. Microwave dielectric ceramics for resonators and filters in mobile phone networks. *J. Am. Ceram. Soc.* **89,** 2063–2072 (2006).
6. Bell, A. J. Ferroelectrics: the role of ceramic science and engineering. *J. Eur. Ceram. Soc.* **28,** 1307–1317 (2008).
7. Ogihara, H., Randall, C. A. & Trolier-McKinstry, S. High-energy density capacitors utilizing 0.7 BaTiO$_3$–0.3 BiScO$_3$ ceramics. *J. Am. Ceram. Soc.* **92,** 1719–1724 (2009).
8. Xiong, B., Hao, H., Zhang, S. J., Liu, H. X. & Cao, M. H. Structure, dielectric properties and temperature stability of BaTiO$_3$–Bi(Mg$_{1/2}$Ti$_{1/2}$)O$_3$ perovskite solid solutions. *J. Am. Ceram. Soc.* **94,** 3412–3417 (2011).
9. Chu, B. J. *et al.* A dielectric polymer with high electric energy density and fast discharge speed. *Science* **313,** 334–336 (2006).
10. Ho, J., Jow, T. R. & Boggs, S. Historical introduction to capacitor technology. *IEEE Electr. Insul. Mag.* **26,** 20–25 (2010).
11. Johnson, R. W., Evans, J. L., Jacobsen, P., Thompson, J. R. & Christopher, M. The changing automotive environment: high-temperature electronics. *IEEE Trans. Electron. Packag. Manuf.* **27,** 164–176 (2004).
12. Watson, J. & Castro, G. High-temperature electronics pose design and reliability challenges. *Analog. Dialog* **46,** 1–7 (2012).
13. Weimer, J. A. Electrical power technology for the more electric aircraft. In *Proc. AIAA/IEEE Digital Avionics Systems Conf.* http://dx.doi.org/10.1109/DASC.1993. 283509 (IEEE, 1993).
14. Rabuffi, M. & Picci, G. Status quo and future prospects for metallized polypropylene energy storage capacitors. *IEEE Trans. Plasma Sci.* **30,** 1939–1942 (2002).
15. Wang, D. H., Kurish, B. A., Treufeld, I., Zhu, L. & Tan, L. S. Synthesis and characterization of high nitrile content polyimides as dielectric films for electrical energy storage. *J. Polym. Sci. A* **53,** 422–436 (2015).
16. Ho, J. & Jow, T. R. High field conduction in heat resistant polymers at elevated temperature for metallized film capacitors. In *Power Modulator and High Voltage Conf.* http://dx.doi.org/10.1109/IPMHVC.2012.6518764 (IEEE, 2012).
17. Venkat, N. *et al.* High temperature polymer film dielectrics for aerospace power conditioning capacitor applications. *Mater. Sci. Eng. B* **168,** 16–21 (2010).
18. Tan, D., Zhang, L. L., Chen, Q. & Irwin, P. High-temperature capacitor polymer films. *J. Electron. Mater.* **43,** 4569–4575 (2014).
19. Pan, J. L., Li, K., Chuayprakong, S., Hsu, T. & Wang, Q. High-temperature poly(phthalazinone ether ketone) thin films for dielectric energy storage. *ACS Appl. Mater. Interf.* **2,** 1286–1289 (2010).
20. Dean, C. R. *et al.* Boron nitride substrates for high-quality graphene electronics. *Nature Nanotechnol.* **5,** 722–726 (2010).
21. Sevik, C., Kinaci, A., Haskins, J. B. & Çağın, T. Characterization of thermal transport in low-dimensional boron nitride nanostructures. *Phys. Rev. B* **84,** 085409 (2011).
22. Coleman, J. N. *et al.* Two-dimensional nanosheets produced by liquid exfoliation of layered materials. *Science* **331,** 568–571 (2011).
23. Ieda, M. Dielectric breakdown process of polymers. *IEEE Trans. Electr. Insul.* **15,** 206–224 (1980).
24. Li, Q. *et al.* Solution-processed ferroelectric terpolymer nanocomposites with high breakdown strength and energy density utilizing boron nitride nanosheets. *Energy Environ. Sci.* **8,** 922–931 (2015).
25. Dang, Z. M., Yuan, J., Yao, S. H. & Liao, R. J. Flexible nanodielectric materials with high permittivity for power energy storage. *Adv. Mater.* **25,** 6334–6365 (2013).
26. Montanari, D. *et al.* Film capacitors for automotive and industrial applications. In *Proc. CARTS USA* 23–38 (Electronic Components Industry Association, 2009).
27. O'Dwyer, J. J. *The Theory of Electrical Conduction and Breakdown in Solid Dielectrics* Ch. 1 (Clarendon, 1973).
28. Qin, S., Ho, J., Rabuffi, M., Borelli, G. & Jow, T. R. Implications of the anisotropic thermal conductivity of capacitor windings. *IEEE Electr. Insul. Mag.* **27,** 7–13 (2011).
29. Zebouchi, N. *et al.* Electrical breakdown theories applied to polyethylene terephthalate films under the combined effects of pressure and temperature. *J. Appl. Phys.* **79,** 2497–2501 (1996).
30. Mark, J. E. *Physical Properties of Polymers Handbook* Ch.10 (AIP Press, 1996).

METHODS

Materials. Dipropylene glycol dimethyl ether (DMM), BCB monomers and b-staged BCBs (partially polymerized) with the number average molecular weight of ~25,000 were provided by Dow Chemical. Boron nitride powders were purchased from Sigma-Aldrich. The high-T_g polymer dielectric films were provided by PolyK Technologies. The polyimide (Kapton) films were vacuum dried overnight at 70 °C before use. All the other materials were used as received.

Preparation. BNNSs were prepared from boron nitride powders using a solution phase exfoliation method[22]. To make the nanocomposites, BNNSs were first dispersed in DMM at a concentration of 5 mg ml^{-1}. 100 mg of BCB monomers were dissolved in 2 ml of DMM and stirred for 2 h. Afterwards the DMM solution of BNNSs was mixed with BCB solution in proportion, and the mixture was first stirred for 10 min and then sonicated for 5 min using a tip-type sonicator (175 W). To crosslink the material, the mixture was drop-cast on a glass slide and subject to baking at 120 °C for 30 min, which was followed by curing at 250 °C for 2 h under N$_2$. The film was peeled off after soaking in water for 5 min. The film thickness can be varied by tuning the concentration of the cast solution. The thickness of films used for electrical characterizations is within the range of 6–12 μm. For ultraviolet-induced crosslinking of the material, DMM solution of b-staged BCB mixed with BNNSs was used to cast a film on Si wafer by spin-coating. Then the spin-coated film was subject to a 20-min ultraviolet exposure in an ultraviolet crosslinker (XL-1500, Spectroline) equipped with ultraviolet tubes (BLE-1T155, Spectroline). The thickness of the film can be varied by changing the solution concentration and parameters of spin-coating. Typically, a 30 wt% solution spin-coated at 700 r.p.m. yields a 4-μm-thick film, which, after curing at 250 °C for 15 min under N$_2$, achieves the same level of performance as that of the thermally crosslinked films. For a typical procedure of photopatterning, the material was spin-coated on Si wafer from a 20 wt% solution of b-staged BCB mixed with BNNSs at 3,000 r.p.m., and then covered with an optical mask before ultraviolet irradiation. Afterwards, the material was developed using DMM and dried.

Characterization. Fourier-transform infrared (FTIR) spectra were obtained in the attenuated total reflectance (ATR) mode using a ZnSe crystal as a contact to the samples with a Varian Digilab FTS-8010 spectrometer. Differential scanning calorimetry was conducted by using a TA Instrument Q100 differential scanning calorimeter at a heating/cooling rate of 10 °C min^{-1}. X-ray diffraction analysis was studied using a PANalytical X'pert Pro MPD theta-theta diffractometer. Thermogravimetric analysis was performed with a TGA 2050 Analyzer at a heating rate of 10 °C min^{-1}. TEM images were obtained on a JEOL JEM-2001F transmission electron microscope. Scanning electron microscopy measurements were performed with a FEI Nova NanoSEM 630 field emission electron microscope. Gold electrodes of diameter 6 mm and thickness 60 nm were sputtered on both sides of the polymer films for the electrical measurements. Dielectric spectra were acquired over a broad temperature range using a Hewlett Packard 4284A LCR meter in conjunction with a Delta Design oven model 2300. Dielectric spectra under direct current bias were collected with the same equipment along with a Hewlett Packard 4140B pA meter/voltage source, a KEPCO BOP 1000M amplifier and a protective circuit. Conduction currents were obtained under an electric field provided by a Hewlett Packard 4140B pA meter/voltage source and TREK model 2210 amplifier. High-field electric displacement–electric field loops were collected using a modified Sawyer–Tower circuit, where the samples were subject to a triangular unipolar wave with a frequency of 10 Hz. Dielectric breakdown strength measurements were performed on a TREK P0621P instrument using the electrostatic pull-down method under a direct-current voltage ramp of 500 V s^{-1}. Young's moduli were derived from strain–stress curves measured with a TA RSA-G2 Solids Analyzer, using a constant linear stretching rate of 0.02% s^{-1}.

See Supplementary Information section 6 for the method of thermal conductivity measurement.

Two-parameter Weibull statistic. Dielectric breakdown strength is analysed within the framework of a two-parameter Weibull statistic described as:

$$P(E) = 1 - \exp(-(E/\alpha)^{\beta})$$

where $P(E)$ is the cumulative probability of electric failure, E is the measured breakdown field, the scale parameter α is the field strength for which there is a 63% probability for the sample to breakdown (Weibull breakdown strength), the shape parameter β evaluates the scatter of data and a higher value of β represents greater dielectric reliability.

Temperature coefficient of dielectric constant. The temperature coefficient of dielectric constant, τ_{ε_r}, for a given temperature range (from T_i to T_f), is defined as:

$$\tau_{\varepsilon_r} = (K_f - K_i)/[K_{ref}(T_f - T_i)]$$

where K_{ref} is the dielectric constant at room temperature, T_i and T_f are the low-end and high-end temperatures, respectively, and K_i and K_f are the dielectric constants at T_i and T_f, respectively.

Simulation of steady-state temperature distribution. The full-field temperature evolution in the metallized thin film capacitor during joule heating is mathematically governed by

$$\rho_m C \frac{\partial T(\boldsymbol{x})}{\partial t} = K \nabla^2 T(\boldsymbol{x}) + \sigma(\boldsymbol{x}, T) E^2 \quad (1)$$

where ρ_m and C are the density and heat capacity respectively. K is the thermal conductivity and E stands for the applied electrical field. In particular, as shown by the experimental measurements, the electrical conductivity σ depends on the temperature T, having the characteristic form of:

$$\sigma = \sigma_0 \exp\left(-\frac{A}{k_B T}\right) \quad (2)$$

where the coefficients σ_0 and A for each material at one specific applied electric field are calculated by fitting the measured data and k_B is the Boltzmann constant. Setting $\partial T(\boldsymbol{x})/\partial t = 0$ yields the steady-state temperature solution of equation (1):

$$K \nabla^2 T(\boldsymbol{x}) + \sigma(\boldsymbol{x}, T) E^2 = 0 \quad (3)$$

The governing equation is then solved by finite element simulations using the commercial software Comsol 5.0 (http://www.comsol.com/release/5.0). When the capacitor is operating the thin slices of the structures are packed into an enclosure, with the cooling liquid surrounding the enclosure. Therefore, the capacitor is treated as an integrated body with a uniform applied electric field for each calculation. The geometries arising from the experimental setup are used in the finite element model. As a result of the laminar structure of the capacitor, in which the polymer has a relatively low thermal conductivity compared to the metallization, the anisotropy in thermal the conductivity is considered in the model (as shown in Supplementary Information section 6). During the finite element simulation, the heat flux at all the enclosure surfaces of the capacitor is produced by both convective and radiative heat transfer arising from the surrounding cooling, with the form:

$$\boldsymbol{n}(-K\nabla T) = h(T - T_{ext}) + \sigma_{SB}\varepsilon(T^4 - T_{ext}^4) \quad (4)$$

where T_{ext} is the surrounding temperature, h is convective heat transfer coefficient, σ_{SB} is the Stefan–Boltzmann constant, and ε is the emissivity of the surfaces. Owing to symmetry only 1/8 of the volume is modelled. Based on the mesh-sensitive study, the number of mesh elements in the system is set as $120 \times 120 \times 30$ with a grid spacing of 0.33 mm.